J|A|C|S ARTICLES

Published on Web 02/09/2010

A Combined Solid-State NMR and Synchrotron X-ray Diffraction Powder Study on the Structure of the Antioxidant (+)-Catechin 4.5-hydrate.

James K. Harper,[†] Jennifer A. Doebbler,[‡] Elisabeth Jacques,[†] David M. Grant,*[,†] and Robert B. Von Dreele[‡]

Department of Chemistry, University of Utah, 315 South 1400 East, Salt Lake City, Utah 84112, and Argonne National Laboratory, Advanced Photon Source, 9700 South Cass Avenue, Argonne, Illinois 60439

Received September 9, 2009; E-mail: grant@chem.utah.edu

Abstract: Analyses combining X-ray powder diffraction (XRD) and solid-state NMR (SSNMR) data can now provide crystal structures in challenging powders that are inaccessible by traditional methods. The flavonoid catechin is an ideal candidate for these methods, as it has eluded crystallographic characterization despite extensive study. Catechin was first described nearly two centuries ago, and its powders exhibit numerous levels of hydration. Here, synchrotron XRD data provide all heavy-atom positions in (+)-catechin 4.5-hydrate and establish the space group as *C*2. SSNMR data (^{13}C tensor and ^{1}H/^{13}C correlation) complete the conformation by providing catechin's five OH hydrogen orientations. Since 1903, this phase has been erroneously identified as a 4.0 hydrate, but XRD and density data establish that this discrepancy is due to the facile loss of the water molecule located at a Wyckoff special position in the unit cell. A final improvement to heavy-atom positions is provided by a geometry optimization of bond lengths and valence angles with XRD torsion angles held constant. The structural enhancement in this final structure is confirmed by the significantly improved fit of computed ^{13}C tensors to experimental data.

Introduction

Flavonoids are a group of phytochemicals that are, perhaps, best known for their antioxidant properties. These nonessential nutrients relieve oxidative stress from both metabolic and exogenous sources, which can lead to aging and disorders such as heart disease and cancer.[1] The flavonoids have considerable structural diversity that corresponds with a wide variety of other bioactivities. Certain flavonoids exhibit antitumor[2] and insecticidal[3] activities, and some appear to play an important role in maintaining ecosystems.[4] The Dictionary of Natural Products lists 6805 known flavonoids in 82 subclasses;[5] while the majority of these compounds have been well characterized using various analytical or synthetic methods, nearly 85% have no reported crystal structures. Since the majority of the flavonoids are bioactive, the availability of more crystal structures promises to extend our understanding of the mechanism of their activity.

In this paper, we report a combined solid-state NMR/X-ray powder diffraction (SSNMR/XRD) analysis for one of the simplest monomeric flavonoids, (+)-catechin ($C_{15}O_6H_{14}$, shown in Figure 1). Catechin belongs to the subclass flavan-3-ols[5] and occurs naturally in green tea leaves,[6] wine,[7] certain fruits and seeds,[8] and chocolate.[9] The presence of catechin in wine may help explain the "French Paradox"—a low incidence of heart disease despite a diet rich in high-fat foods. Catechin has also been shown to block the growth of human cell lines originating from prostate[10] and breast[11] cancers. In addition to its antioxi-

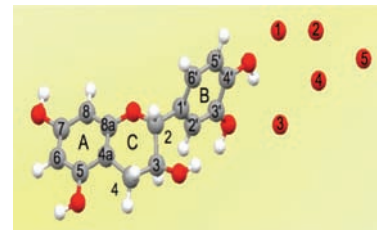

Figure 1. Structure of catechin showing the crystallographic asymmetric unit with the carbon and water oxygen numbering used herein. Individual rings are designated by letters as shown.

[†] University of Utah.
[‡] Argonne National Laboratory.

(1) Dani, C.; Bonatto, D.; Salvador, M.; Pereira, M. D.; Henriques, J. A.; Eleutherio, E. *J. Agric. Food Chem.* **2008**, *56*, 4268.
(2) Kanadaswami, C.; Lee, L.-T.; Lee, P.-P. H.; Hwang, J.-J.; Ke, F.-C.; Huang, Y.-T.; Lee, M.-T. *In Vivo* **2005**, *19*, 895.
(3) Sosa, M. E.; Tonn, C. E. *Phytochem. Rev.* **2007**, *7*, 3.
(4) (a) Feeny, P. P. *Phytochemistry* **1969**, *8*, 2119. (b) Feeny, P. P. *Ecology* **1970**, *51*, 565. (c) Rhodes, D. F. In *Herbivores-Their Interactions with Secondary Plant Metabolites*; Janzen, D. H., Rosenthal, G. A., Eds.; Academic Press: London, New York, 1979; p 3.
(5) *Dictionary of Natural Products*; Buckingham, J., Ed.; Chapman & Hall: London, 1994; Vol. 7, pp 94−134.
(6) Nonaka, G.; Kawahara, O.; Nishioka, I. *Chem. Pharm. Bull.* **1983**, *31*, 3906.
(7) Leopoldini, M.; Russo, N.; Toscano, M. *J. Agric. Food Chem.* **2007**, *55*, 7944.
(8) Fuecht, W.; Nachit, M. *Mitt. - Hoehere Bundeslehr- Versuchsanst. Wein- Obstbau, Klosterneuberg* **1974**, *24*, 293.
(9) Kofink, M.; Papagiannopoulos, M.; Galensa, R. *Molecules* **2007**, *12*, 1274.
(10) Kampa, M.; Hatzoqlou, N.; Notas, G.; Damianaki, A.; Bakogeorgou, E.; Gemetzi, C.; Kouroumalis, E.; Martin, P.-M.; Castanas, E. *Nutr. Cancer* **2000**, *37*, 223.

10.1021/ja907671p

dant and anticancer activities, catechin is antimutagenic[12] and has been implicated in the therapeutic treatment of liver disease.[13]

Catechin was originally described nearly two centuries ago[14] and has been the focus of an enormous amount of research.[15] Despite this intense emphasis and catechin's relatively rigid structure, which would seem to favor crystal formation, no crystal structure has yet been reported. Many conformational conclusions regarding flavan-3-ols are therefore presumed from crystal structures of catechin derivatives such as 6-bromo-3,3′,4′,5,7-penta-*O*-methylcatechin,[16] 8-bromo-tetra-*O*-methyl-(+)-catechin,[17] penta-*O*-acetyl-(+)-catechin,[18] and tetra-*O*-methyl-(+)-catechin[19] or closely related products such as epicatechin.[20] However, the relevance of structures derived from related products may be debated, since these structures have steric and/or stereochemical differences. The potential for discrepancy is illustrated by the observation of an axial orientation of the B ring in penta-*O*-acetyl-(+)-catechin—a conformation unique among the characterized derivatives. Other methods have been applied to catechin, including theoretical[21] and SSNMR[22] to predict structure, but these studies provided no information on the crystal structure.

The limited insight provided from existing single-crystal diffraction studies of products related to catechin has motivated research on the microcrystalline phases of catechin using powder diffraction methods. Presently, six microcrystalline forms of (+)-catechin are known: a tetrahydrate, two monohydrates, and three anhydrates.[23] Differences in the powder diffraction patterns for all six forms have been demonstrated, but further crystallographic information is unavailable. In this study, we extend these powder studies to provide a full crystal structure for the tetrahydrate using SSNMR and synchrotron XRD with a high-resolution multianalyzer diffractometer.

X-ray powder diffraction and SSNMR have become prominent techniques for analyzing microcrystalline powders. Both methods have the advantage of providing structural information on individual atomic sites, which can be used to provide complete structures: generally for small molecules but also small proteins.[24,25] The potential for these techniques to characterize hydrogen bonding is particularly interesting, because the binding of small molecules by receptors is frequently directed by hydrogen bonding.[26] However, crystal structures provide significantly more insight than just atomic positions: for example, optical properties, magnetic susceptibility, and electrical conductivity of certain solids can also be predicted.[27]

Recently, our groups and others have employed a combination of SSNMR and XRD to provide full crystal structures for several compounds.[28] Synchrotron data are particularly helpful in these studies, due to the higher resolution and increased signal-to-noise ratio. This combination of SSNMR and XRD techniques overcomes some of the weaknesses of either method used alone, such as the challenges to XRD created by overlap of Bragg peaks or the difficulty for many SSNMR methods to characterize long-range order. Various approaches have been proposed for combining SSNMR and XRD data,[28] and the availability of these methods invites application to classes of solids that have historically been difficult to study. Recently, characterization of certain problematic zeolites has been demonstrated using these techniques.[28a,h,29] In these materials, the connectivity in the basic repeating structural unit is provided by a SSNMR pulse sequence developed to measure $^{29}Si/^{29}Si$ distances.[30] This initial SSNMR model structure serves as a starting point for the full

(11) Damianaki, A.; Bakogeorgou, E.; Kampa, M.; Notas, G.; Hatzoglou, A.; Panagiotou, S.; Gemitzi, C.; Kouroumalis, E.; Martin, P.-M.; Castanas, E. *J. Cell. Biochem.* **2000**, *78*, 429.
(12) Hayatsu, H.; Negishi, T.; Arimoto, S. *Basic Life Sci.* **1993**, *61*, 387.
(13) (a) Aguilar, R. J.; de la Santa, L. J.; Cuadras, A. C. M.; Kern, A. *Fortschr. Med.* **1978**, *92*, 75. (b) Blum, A. L.; Berthet, P.; Doelle, W.; Goebell, H.; Kortum, K.; Pelloni, S.; Peter, P.; Poulsen, H.; Strohmeyer, G.; Tygstrup, N. *Lancet* **1977**, *2*, 1153.
(14) Runge, F. F. *Neueste Phytochemische Entdeckungen zur Begründung einer Wissenschaft; Lieferungen: Berlin* **1821**, 245.
(15) Representative references include: (a) Rice-Evans, C. A.; Miller, N. J.; Paganga, G. *Trends Plant Sci.* **1997**, *2*, 152. (b) Kandaswami, C.; Middleton, E. In *Natural Antioxidants, Chemistry, Health Effects, and Applications*; Shahidi, F., Ed.; AOAC Press: Champaign, IL, 1997; pp 174−203. (c) Li, W.; Sun, G. Y. In *Biological Oxidants and Antioxidants. Molecular Mechanisms and Health Effects*; Packer, L., Ong, O. S. H., Eds.; AOAC Press: Champaign, IL, 1998; pp 90−103. (d) Cook, N. C.; Samman, S. *J. Nutr. Biochem.* **1996**, *7*, 66. (e) Formica, J. V.; Regelson, W. *Food Chem. Toxicol.* **1995**, *33*, 1061. (f) Lopez-Lazaro, M. *Curr. Med. Chem.: Anti-Cancer Agents* **2002**, *2*, 691. (g) Wang, H. K. *Expert Opin. Invest. Drugs* **2000**, *9*, 2103. (h) Hayatsu, H.; Negishi, T.; Arimoto, S. *Basic Life Sci.* **1993**, *61*, 387. (i) Kajiya, K.; Kumazawa, S.; Nakayama, T. *Biosci. Biotechnol. Biochem.* **2001**, *65*, 2638.
(16) Einstein, F. W. B.; Kiehlmann, E.; Wolowidnyk, E. K. *Can. J. Chem.* **1985**, *63*, 2176.
(17) Engel, D. W.; Hattingh, M.; Hundt, H. K. L.; Roux, D. G. *J. Chem. Soc., Chem. Commun.* **1978**, 695.
(18) Fronczek, F. R.; Gannuch, G.; Mattice, W. L.; Hemingway, R. W.; Chiari, G.; Tobiason, F. L.; Houglum, K.; Shanafelt, A. *J. Chem. Soc., Perkin Trans. 2* **1985**, 1383.
(19) Fronczek, F. R.; Hemingway, R. W.; McGraw, G. W.; Steynburg, J. P.; Helfer, C. A.; Mattice, W. L. *Biopolymers* **1993**, *33*, 275.
(20) (a) Spek, A. L.; Kojic-Prodic, B.; Labadie, R. P. *Acta Crystallogr.* **1984**, *C40*, 2068. (b) Fronczek, F. R.; Gannuch, G.; Mattice, W. L.; Tobiason, F. L.; Broeker, J. L.; Hemingway, R. W. *J. Chem. Soc., Perkin Trans. 2* **1984**, 1611.
(21) Leopoldini, M.; Russo, N.; Toscano, M. *J. Agric. Food Chem.* **2007**, *55*, 7944.
(22) Harper, J. K.; Strohmeier, M.; Grant, D. M. *J. Magn. Reson.* **2007**, *189*, 20.
(23) Marti, E.; Heiber, O.; Gumma, A.; Huber, G.; Utsumi, I.; Nakagawa, H.; Miyata, T.; Akimoto, K. U.S. Patent4,515,804; 1985.
(24) Von Dreele, R. B. *J. Appl. Crystallogr.* **1999**, *32*, 1084.
(25) (a) Rienstra, C. M.; Tucker-Kellogg, L.; Jaroniec, C. P.; Hohwy, M.; Reif, M. T.; McMahon, B. T.; Lozano-Pérez, T.; Griffin, R. G. *Proc. Natl. Acad. Sci. U.S.A.* **2002**, *99*, 10260. (b) Castellani, F.; van Rossum, B.-J.; Diehl, A.; Schubert, M.; Oschkinat, H. *Nature* **2002**, *420*, 98. (c) Jaroni, C. P.; MacPhee, C. E.; Bajaj, V. S.; McMahon, M. T.; Dobson, C. M.; Griffin, R. G. *Proc. Natl. Acad. Sci. U.S.A.* **2003**, *101*, 711.
(26) (a) Hubbard, R. E. In *Handbook of Proteins*; Cox, M. M., Phillips, G. N., Eds.; Wiley: Chichester, U.K., 2007; Vol. 1, pp 32−37. (b) Coulocheri, S. A.; Pigis, D. G.; Pappavassiliou, K. A.; Papavassiliou, A. G. *Biochimie* **2007**, *89*, 1291. (c) Kool, E. T. *Annu. Rev. Biophys. Biomol. Struct.* **2001**, *30*, 1. (d) Fujiki, M.; Saxena, A. *J. Polym. Sci., Part A: Polym. Chem.* **2008**, *46*, 4637.
(27) Bhagavantam, S. *Crystal Symmetry and Physical Properties*; Academic Press: London, 1966.
(28) (a) Brouwer, D. H.; Darton, R. J.; Morris, R. E.; Levitt, M. H. *J. Am. Chem. Soc.* **2005**, *127*, 10365. (b) Dutour, J.; Guillou, N.; Huguenard, C.; Taulelle, F.; Mellot-Draznieks, C.; Férey, G. *Solid State Sci.* **2004**, *6*, 1059. (c) Rajeswaren, M.; Blanton, T. N.; Zumbulyadis, N.; Giesen, D. J.; Conesa-Moratilla, C.; Misture, S. T.; Stephens, P. W.; Huq, A. *J. Am. Chem. Soc.* **2002**, *124*, 14450. (d) Middleton, D. A.; Peng, X.; Saunders, D.; Shankland, K.; David, W. I. F.; Markvardsen, A. J. *Chem. Commun.* **2002**, 1976. (e) Harper, J. K.; Grant, D. M.; Zhang, Y.; Lee, P. L.; Von Dreele, R. *J. Am. Chem. Soc.* **2006**, *128*, 1547. (f) Harris, R. K.; Ghi, P. Y.; Hammond, R. B.; Ma, C. Y.; Roberts, K. J.; Yates, J. R.; Pickard, C. J. *Magn. Reson. Chem.* **2006**, *44*, 325. (g) Smith, E. D. L.; Hammond, R. B.; Jones, M. J.; Roberts, K. J.; Mitchell, J. B. O.; Price, S. L.; Harris, R. K.; Apperley, D. C.; Cherryman, J. C.; Docherty, R. *J. Chem. Phys. B* **2001**, *105*, 5818. (h) Brouwer, D. H. *J. Am. Chem. Soc.* **2008**, *130*, 6306. (i) King, I. J.; Fayon, F.; Massiot, D.; Harris, R. K.; Evans, J. S. O. *Chem. Commun.* **2001**, 1766. (j) Witter, R.; Sternberg, U.; Hesse, S.; Kondo, T.; Koch, F. T.; Ulrich, A. S. *Macromolecules* **2006**, *39*, 6125.
(29) Brouwer, D. H.; Enright, G. J. *J. Am. Chem. Soc.* **2008**, *130*, 3095.
(30) Brouwer, D. H.; Kristiansen, P. E.; Fyfe, C. A.; Levitt, M. H. *J. Am. Chem. Soc.* **2005**, *127*, 542.

crystallographic characterization by XRD. These refinements have recently been improved by including ^{29}Si tensor principal value data to provide structures rivaling those obtained by single-crystal X-ray diffraction.[28h] This pioneering work on zeolites portends similar applications to other classes of materials. Here, an extension of these techniques is reported using ^{13}C SSNMR data and synchrotron XRD data in parallel to evaluate the flavonoid catechin.

Experimental Section

(+)-Catechin powder (290.27 g/mol) was purchased from Fluka and recrystallized in HPLC grade water by adding approximately 25 mL of water to 5 g of catechin. This procedure has been used for over a century to yield a microcrystalline phase known as the tetrahydrate.[31] The recrystallization steps were repeated twice more to ensure high sample purity. A small amount of water was retained in the sample, since fully drying the powder causes a phase change to the β-monohydrate form within 1 day, even at room temperature. This procedure was also followed to prepare the sample recrystallized from D_2O, with 99.9% deuterium D_2O (Cambridge Isotope Laboratories) replacing the HPLC grade water.

The density of (+)-catechin recrystallized from H_2O was measured to be 1.449 g/cm^3 by the floatation method using a mixture of bromobenzene and chlorobenzene. The sample was prepared by pouring the catechin/water slurry onto filter paper and then allowing most of the water to dry through a wicking process over a 1−2 h period. This procedure retains all water molecules in the lattice and simply removes water not associated with the lattice, as demonstrated by the close match between an isotropic ^{13}C SSNMR spectrum of this sample and a spectrum from a freshly prepared sample. The theoretical density of catechin 4.5-hydrate (1.456 g/cm^3) provides the best match to the experimental density with an error of only +0.48%.

Powder data were collected at the new powder diffraction beamline (11-BM) at the Advanced Photon Source, Argonne National Laboratory,[32] at 15 keV (λ = 0.8133 Å), with the sample spun at 5400 rpm to ensure powder averaging. Calibration of the instrument for wavelength, detector offsets, and instrument profile shapes was performed with a mixture of NIST SRMs 640c (Si), 676a (Al_2O_3), 660a (LaB_6), and sucrose (Domino sugar). Data were typically collected from −6 to 80° at 0.05 or 0.01 s/step with 0.001° steps.

The hydrated catechin powder was packed into a Kapton capillary tube following the standard protocol for protein samples.[33] Four individual data sets at the same sample location were taken from −6 to 50° with 0.001° steps at 0.01 s/step, resulting in collection times of 9.3 min per data set. These rapid analyses of samples packed in sealed capillaries ensured that all waters of hydration were retained in the lattice. The first data set alone was used for both the Pawley refinement and the molecular replacement calculations. Once the molecular replacement solution was determined, all four data sets were combined in order to increase the signal-to-noise ratio and improve the data quality.

The SSNMR ^{13}C tensor principal value data were collected on a Chemagnetics CMX 400 MHz spectrometer using a 7.5 mm rotor and the FIREMAT pulse sequence[34] with TPPM decoupling.[35] Data were collected using a sample recrystallized from H_2O and then cooled to −15 °C to prevent a phase change to the β-monohydrate. The spectrum was referenced to the high-frequency peak of adamantane at 38.56 ppm, and a sample spinning speed of 813 Hz was used together with a pulse delay of 3 s. Pulse widths of 4.1 μs (^{1}H 90°) and 8.5 μs (^{13}C 180°) were used. Evolution and acquisition dimension spectral widths of 20.325 and 33.333 kHz, respectively, were chosen. The digital resolution in the acquisition dimension was 32.5 Hz/point. Twenty-five evolution points of 192 scans each were collected and the data processed using the replication and rearrangement scheme described elsewhere.[34] A total of 625 evolution data points were generated after replication with a digital resolution of 32.5 Hz/point. An estimation of the average error in experimental principal values was obtained by acquiring a total of three FIREMAT data sets using, for each analysis, the parameters listed above and a new sample of recrystallized catechin. An average error of ±0.9 ppm was determined from these data.

The ^{13}C/^{1}H heteronuclear dipolar correlation (HETCOR) data were acquired on a Varian Infinity plus operating at 599.789 16 and 150.830 70 MHz for ^{1}H and ^{13}C, respectively. Analyses were performed at a spinning speed of 11 kHz using a T3 4 mm probe and the pulse sequence of van Rossum et al.[36] Five data sets were acquired for the catechin sample recrystallized in D_2O using cross-polarization (CP) times of 70, 120, 170, 210, and 300 μs. A sixth data set was acquired to clarify assignments at C6 and C8 using a sample recrystallized from H_2O and a short contact time (90 μs) that emphasized covalently bonded ^{1}H−^{13}C sites. For all data sets, other parameters included 64 evolution increments of 128 scans each, ^{1}H and ^{13}C spectral widths of 23.920 and 30.003 kHz, respectively, and recycle times of 3.0 s. The intensity of the B_1 (^{1}H) field was 104.2 kHz, and each evolution increment consisted of two Lee−Goldberg 2π cycles. Spectra were externally referenced to TMS (^{1}H) at 0.0 ppm and the high-frequency peak of adamantane (^{13}C) at 38.56 ppm. A ^{1}H scaling factor of 0.828 was determined using a procedure described elsewhere.[37]

Computed tensors were calculated using Gaussian 03[38] at the B3PW91/D95** level of theory.[39] Prior work has demonstrated that B3PW91 calculations provide better matches to experimental ^{13}C tensor data than several alternative methods.[40] Recently, improved procedures for computing shift tensors have been introduced;[41] however, the B3PW91/D95** calculations provided sufficiently accurate tensors to assign dihedral angles with high statistical confidence at all positions examined. A detailed comparison of other tensor computation methods is given elsewhere.[42] We note that the B3PW91 method suffers from systematic errors in the calculation of tensor values[40c] due, perhaps, to its inability to fully account for electron correlation. Other tensor computation methods have also been found to suffer from systematic errors, and methods for compensating for these inaccuracies are described elsewhere.[42c,43] In B3PW91 calculations, this error is primarily evident at sp^2 carbons, where errors are significantly larger than

(31) Clauser, R. *Chem. Ber.* **1903**, *36*, 101.
(32) Wang, J.; Toby, B. H.; Lee, P. L.; Ribaud, L.; Antao, S. M.; Kurtz, C.; Ramanathan, M.; Von Dreele, R. B.; Beno, M. A. *Rev. Sci. Instrum.* **2008**, *79*, 085105.
(33) Von Dreele, R. B. *J. Appl. Crystallogr.* **2006**, *39*, 124.
(34) Alderman, D. W.; McGeorge, G.; Hu, J. Z.; Pugmire, R. J.; Grant, D. M. *Mol. Phys.* **1998**, *95*, 1113.
(35) Bennett, A. E.; Reinstra, C. M.; Auger, M.; Lakshmi, K. V.; Griffin, R. J. *J. Chem. Phys.* **1995**, *103*, 6951.
(36) Van Rossum, B.-J.; Förster, H.; de Groot, H. J. M. *J. Magn. Reson.* **1997**, *124*, 516.
(37) Brus, J.; Jegorov, A. *Phys. Chem. A* **2004**, *108*, 3955.
(38) Frisch, M. J.; Gaussian 03, revision A.9; Gaussian, Inc., Pittsburgh, PA, 2003 (see full reference in the Supporting Information).
(39) (a) Becke, A. D. *J. Chem. Phys.* **1993**, *98*, 5648. (b) Lee, C.; Yang, W.; Parr, R. G. *Phys. Rev. B* **1988**, *37*, 785.
(40) (a) Harper, J. K.; McGeorge, G.; Grant, D. M. *J. Am. Chem. Soc.* **1999**, *121*, 6488. (b) Harper, J. K.; McGeorge, G.; Grant, D. M. *Magn. Reson. Chem.* **1998**, *36*, S135. (c) Harper, J. K. *Encyclopedia of Magnetic Resonance*; Grant, D. M., Harris, R. K., Eds.; Wiley: Chichester, U.K., 2002; Vol. 9, pp 589−597.
(41) (a) Sebastiani, D.; Parrinello, M. *J. Phys. Chem. A* **2001**, *105*, 1951. (b) Pickard, C. J.; Mauri, F. *Phys. Rev. B* **2001**, *63*, 245101. (c) Perdew, J. P.; Burke, K.; Ernzerhof, M. *Phys. Rev. Lett.* **1997**, *78*, 1396. (d) Keal, T. W.; Tozer, D. J. *J. Chem. Phys.* **2003**, *119*, 3015. (e) Teale, A. M.; Tozer, D. J. *Chem. Phys. Lett.* **2004**, *383*, 109. (f) Yates, J. R.; Pickard, C. J.; Mauri, F. *Phys. Rev. B* **2007**, *76*, 24401.
(42) (a) Sefzik, T. H.; Fidler, J. M.; Iuliucci, R. J.; Facelli, J. C. *Magn. Reson. Chem.* **2006**, *44*, 390. (b) Sefzik, T. H.; Turco, D.; Iuliucci, R. J.; Facelli, J. C. *J. Chem. Phys. A* **2005**, *109*, 1180. (c) Johnston, J. C.; Liliucci, R. J.; Facelli, J. C.; Fitzgerald, G.; Mueller, K. T. *J. Chem. Phys.* **2009**, *131*, 144503.
(43) Dumez, J. N.; Pickard, C. J. *J. Chem. Phys.* **2009**, *130*, 104701.

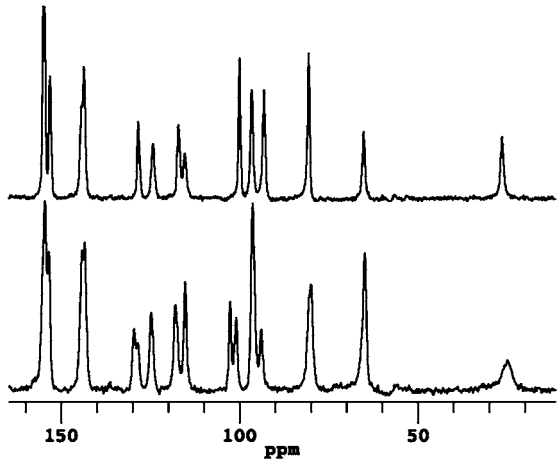

Figure 2. ^{13}C isotropic spectrum of catechin 4.5-hydrate (top plot), establishing that the solid is a single-crystalline phase with one molecule in the asymmetric unit immediately after recrystallization from water. The appearance of new peaks in the bottom spectrum indicates that drying at room temperature, over even short periods of time, produces a second phase.

those found at sp^3 sites. In catechin, this systematic error was largely removed by fitting sp^2 and sp^3 carbons by two separate least-squares procedures. Although this approach has been questioned,[44] the prior demonstration of statistically significant differences in the accuracy of computed tensors at sp^2 and sp^3 sites[40c,42c] justifies separate fittings. All computed and experimental tensor data were converted to the icosahedral representation[45] before using the least-squares fitting procedure. Optimal conversions of shielding values to shifts were achieved using shift = ((shielding) − 185.4781)/−0.9597 for sp^2 sites and shift = ((shielding) − 193.8929)/−1.0945 for sp^3 carbons. Geometry optimizations (B3LYP/D95*)[46] were performed by initially placing the OH hydrogens at the approximate conformations specified by a given model structure and then allowing an unrestricted energy minimization. The B3LYP method with the D95* basis was chosen for the structural refinement because this method has been reported to provide high-quality structures.[47]

Variable-temperature SSNMR ^{13}C data were collected on a Chemagnetics CMX 400 spectrometer using the TOSS pulse sequence[48] with TPPM ^1H decoupling[35] and other parameters as described for the FIREMAT analysis. Reported temperatures are uncalibrated.

Results and Discussion

Preparing a Stable Single Phase of Catechin 4.5-Hydrate. A SSNMR isotropic ^{13}C spectrum of this phase unambiguously established the presence of only one molecule per asymmetric unit with 14 resonances clearly resolved for the 15-carbon structure. Line width and cross-polarization behavior[49] indicated that this phase was crystalline. Sample drying over approximately 1 day, however, induced a phase change to the β-monohydrate form, which was easily discerned by the appearance of new resonance lines (as shown in Figure 2). This change occurred despite the fact that the sample was enclosed in the rotor and the only external effects were from sample spinning and the intermittent application of pulses. This phase change is known to be reversible and strongly dependent on humidity.[23] To prevent this phase change from occurring during analysis, all SSNMR experiments were performed at −15 °C on freshly recrystallized catechin.

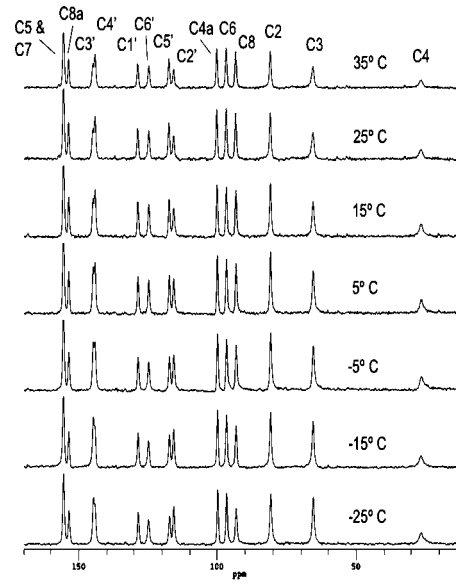

Figure 3. Motion at or near specific molecular sites is seen from changes in ^{13}C line shape over a temperature change of 60 °C. The largest changes in peak shape are observed at C3, C8, C2′, and C3′, indicating dynamic disorder near these sites.

Information regarding molecular motion near specific sites of the molecule was also provided by SSNMR data. Isotropic ^{13}C spectra were acquired over a 60 °C range and changes in resonance intensity and shape noted (as seen in Figure 3). Sample drying during this analysis was avoided by acquiring all data within a 3 h period, and no evidence of a phase change was observed during the analysis, as indicated by the absence of new resonance lines. These data suggest the presence of motion near C3, C8, C2′, and C3′. Subsequent XRD refinement found minimal disorder at these sites, implying that these changes arise from disorder in nearby waters. At all other heavy-atom positions, negligible disorder was also observed, excluding the possibility that catechin exists as a mixture of conformers at non-hydrogen positions.

Assigning ^1H and ^{13}C SSNMR Shifts in Catechin Hydrate. A correct assignment of spectral lines is required for accurate structural analysis. In catechin hydrate, all assignments were made on the basis of $^1H/^{13}C$ HETCOR spectra.[36] Carbon atoms with covalently attached hydrogens were identified from $^1H/^{13}C$ correlations that appeared at contact times less than 100 μs.[50] Correlations appearing at longer contact times served to identify nonprotonated carbons and longer-range $^1H \rightarrow {}^{13}C$ transfers. A complication in the analysis of these spectra arises from the presence of OH hydrogens. These protons give correlations only at longer contact times, because their separation from ^{13}C sites is large compared to protons covalently bound to carbons. This delayed transfer can cause an $O^1H \rightarrow {}^{13}C$ correlation to be mistaken for a long-range $C-{}^1H \rightarrow {}^{13}C$ transfer when the OH proton has a shift value degenerate with a proton

(44) Harris, R. K. *Analyst* **2006**, *131*, 351.
(45) (a) Alderman, D. W.; Sherwood, M. H.; Grant, D. M. *J. Magn. Reson., Ser. A* **1993**, *101*, 188. (b) Grant, D. M.; Halling, M. D. *Concepts Magn. Reson., A* **2009**, *34A*, 217.
(46) Perdew, J. P.; Wang, Y. *Phys. Rev. B* **1992**, *45*, 13244.
(47) Cheeseman, J. R.; Trucks, G. W.; Keith, T. A.; Frisch, M. J. *J. Chem. Phys.* **1996**, *104*, 5497.
(48) Dixon, W. T. *J. Chem. Phys.* **1982**, *77*, 1800.
(49) Offerdahl, T. K.; Salsbury, J. S.; Dong, Z.; Grant, D. J. W.; Schroeder, S. A.; Prakash, I.; Gorman, E. M.; Barich, D. H.; Munson, E. J. *J. Pharm. Sci.* **2005**, *94*, 2591.
(50) Van Rossum, B.-J.; Steengaard, D. B.; Mulder, F. M.; Boender, G. J.; Schaffer, K.; Holzwarth, A. R.; de Groot, H. M. J. *Biochemistry* **2001**, *40*, 1587.

Table 1. Carbon and ^{1}H Chemical Shift Assignments for (+)-Catechin 4.5-Hydrate

position	^{13}C (ppm)	^{1}H (ppm)	^{1}H → ^{13}C correlation
2	81.37	4.4	C2-*H* to C3,[a] C8a,[b] C1′,[a] and C6′[d]
3	66.07	4.2	C3-*H* to C2,[a] C4,[b] C4a,[b] C1′[b], and C2′[a]
		4.8 (C3O-H)	C3O-*H* to C3[a]
4	27.40	1.6, 2.4	C4-*H* to C2,[c] C3,[a] and C4a[a]
4a	100.52		
5	155.81	8.4 (C5O-H)	C5O-*H* to C5[b] and C6[e]
6	97.25	6.1	C6-*H* to C5[e] and C7[e]
7	155.80	9.3 (C7O-H)	C7O-*H* to C7[b] and C8[e]
8	93.79	5.5	C8-*H* to C7[e] and C8a[e]
8a	153.85		
1′	128.97		
2′	116.19	6.3	C2′-*H* to C2,[a] C3,[a] C1′,[a] and C3′[a]
3′	145.12	8.0 (C3′O-H)	C3′O-*H* to C2′[c] and C3′[b]
4′	144.43	9.3 (C4′O-H)	C4′O-*H* to C4′[b]
5′	117.76	5.6	C5′-*H* to C4′[a] and C6′[a]
6′	125.31	5.7	C6′-*H* to C2,[a], C1′,[a] and C5′[a]

[a] Correlation that was best observed at a cross-polarization contact time of 120 μs using a sample recrystallized three times from D_2O. [b] Correlation that was best observed at a cross-polarization contact time of 170 μs using a sample recrystallized three times from D_2O. [c] Correlation that was best observed at a cross-polarization contact time of 210 μs using a sample recrystallized three times from D_2O. [d] Correlation that was best observed at a cross-polarization contact time of 300 μs using a sample recrystallized three times from D_2O. [e] Correlations only observable in a sample recrystallized from H_2O. All correlations were observed at a cross-polarization contact time of 90 μs.

bonded to carbon. Such ^{1}H degeneracies are more common in solid-state spectra than may be anticipated, due to the wide ^{1}H line width in typical spectra. In catechin hydrate, this problem is especially evident because water hydrogens can also produce HO−^{1}H → ^{13}C correlations. To eliminate all O^{1}H → ^{13}C correlations, a sample of catechin was recrystallized from D_2O to convert OH sites to OD and to eliminate H_2O. NMR analysis of the D_2O-containing sample provided clear correlations for most positions, allowing chemical shift assignment. Surprisingly, a small fraction of COH sites remained after D_2O exchange and CO−^{1}H → ^{13}C signals were observed for these sites and provide ^{1}H assignments at the OH groups at C3, C5, C7, C3′, and C4′. Complete ^{1}H and ^{13}C assignments and observed correlations are summarized in Table 1.

The near-degeneracy of ^{1}H shifts at C2 and C3 complicated the shift assignments. Likewise, ^{1}H degeneracy at C5′ and C6′ was observed, as shown in the lower plot of Figure 4. Assignments for the correlations C3−H → C2′, C2−H → C1′, C5′-H → C4′, and C6′-H → C1′ could, however, be made by recognizing that magnetization transfers occur via dipolar coupling that strongly favors the closest hydrogen. Therefore, the degeneracy of the hydrogens at C5′ and C6′, for example, can be readily differentiated in an interaction with C4′, since the proton at C5′ is closer to C4′ and the observed correlation must therefore be assigned as C5′-H → C4′.

Inspection of the ^{13}C spectrum of the D_2O-recrystallized catechin revealed that the signals for C6 and C8 diminished by roughly 50% relative to a sample prepared from H_2O. The low intensity of the C6 and C8 signals resulted in an absence of correlations in the HETCOR spectra of the D_2O-containing sample (Figure 4, top spectrum) and an inability to assign these signals. To correct this omission, a sample recrystallized from H_2O was prepared and analyzed by the HETCOR method. Several missing correlations involving the A-ring were observed in this sample, completing the assignments (Table 1). Corresponding solution shifts support the assignments given with rms deviations between SSNMR and solution shifts of 1.64 ppm for ^{13}C and 0.7 ppm for ^{1}H. Solution shifts were measured in a D_2O solution to provide a direct comparison to the work described herein.[51] All solution shifts in D_2O are available as Supporting Information.

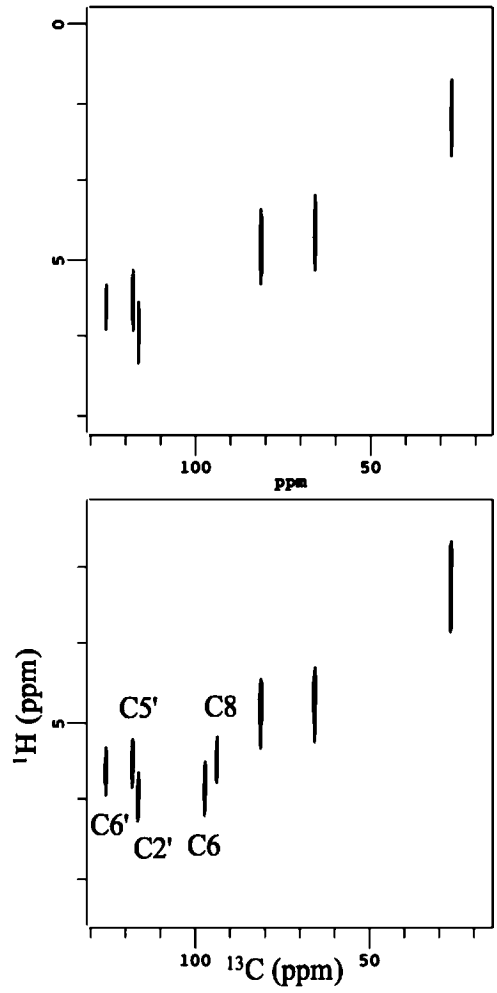

Figure 4. ^{1}H/^{13}C correlation spectra of catechin showing only protons directly bonded to ^{13}C sites, as observed at short contact times of <100 μs. The upper and lower spectra show catechin samples recrystallized from D_2O and H_2O, respectively. The missing C6 and C8 signals in the upper (D_2O) plot facilitate assignments by eliminating ^{1}H degeneracy of the protons from C2′, C5′, and C6′ with those at C6 and C8. In addition, the loss of these correlations indicates that C6 and C8 receive significant cross-polarization contributions from the OH protons at C5 and C7, even at short cross-polarization times. This elimination suggests that the C5 and C7 OH hydrogens are oriented toward C6 and C8, respectively.

The observation that recrystallization from D_2O influences cross-polarization at C6 and C8 suggests conformations for two OH protons. Specifically, the OH to OD conversion at C5 and C7 is expected to modify cross-polarization at C6 and C8 only if these OH protons are oriented directly toward C6 and C8. The only conformation matching this description has an A-ring conformation with the C5 OH proton directed toward C6 and the C7 OH oriented toward C8. Additional SSNMR analyses, described below, confirm these conclusions.

The recrystallization from H_2O generates a solid expected to contain HO ^{1}H → ^{13}C correlations. The presence of such signals provides information needed to map the hydrogen-bonding network involving the water molecules of the asymmetric unit.

(51) Jacques, E. NMR Study of the Complexation of (+)-Catechin and Caffeine; Senior Honors Thesis, University of Utah, 2006.

Unfortunately, only four hydrogens from water were clearly evident as unique shifts and showed water protons near C6, C3′, C5′, and C6′. Presumably, motion at the other water sites is sufficiently rapid to prevent cross-polarization. Hence, only a limited picture of the water hydrogen-bonding network was obtained from SSNMR data.

Synchrotron XRD and Crystal Structure Solution of the Powder Catechin Sample. Structural analysis by XRD can be pursued solely from diffraction data where sufficient resolution is available. However, in many cases an initial structural model is required. This model can be a related molecule or a partial structure. Previously, our group and others have proposed generating this initial model from SSNMR analysis.[28] In the case of catechin, however, a closely related molecule, tetra-*O*-methyl-(+)-catechin,[19] had already been characterized crystallographically, allowing us to employ the classical crystallography method of molecular replacement. A truncated version of tetra-*O*-methyl-(+)-catechin was used as the starting model.

Molecular Replacement via Monte Carlo and Simulated Annealing. The synchrotron X-ray diffraction data set was analyzed in TOPAS (Bruker-AXS) to determine the space group as *C*2 with unit cell parameters $a = 22.17$ Å, $b = 4.71$ Å, $c = 20.16$ Å, and $\beta = 126.40°$. A set of powder structure factors needed for the subsequent molecular replacement was obtained via a Pawley refinement[52] with GSAS[53] over the full *d*-spacing range of 23.3−0.96 Å. A 10-term log linear interpolation function was used to describe the background, and the peak profile function[54] included microstrain broadening terms. The refinement converged to wRp = 0.17 for 873 reflections.

PSSP is a combined Monte Carlo and simulated annealing algorithm,[55] which facilitates molecular replacement of powder diffraction data by accounting for peak overlaps. This software was used to orient the model structure (i.e., the atomic coordinates of tetra-*O*-methyl-(+)-catechin, with all of the methyl groups and hydrogen atoms removed) into the *C*2 unit cell. As the space group for catechin (*C*2) is polar, only two coordinates (*x* and *z*) and three orientations (Eulerian ω, χ, and ϕ) needed to be determined. Fifteen trials using the 150 lowest order reflections were carried out on an annealing schedule of 50−0.001° in 20% decrements, with 50 000 cycles at each "temperature". All of the solutions were identical, but the intermolecular packing was not optimal—most likely due to the high texture of the sample, which preferentially affects the low-order reflections. The hydrogen atoms from the model structure were reintroduced to aid in scattering and prevent close contacts. The range of reflections was reduced to 5.1−30° (9.14−1.57 Å) in an effort to curb any possible texture contribution. The algorithm was rerun with the new set of 150 lowest order reflections over 5 experiments, yielding reasonable packing interactions with all solutions identical.

This final molecular replacement solution provided input to GSAS to begin crystal structure refinement of (+)-catechin. The poor fit in the low-angle regime confirmed the presence of texture, resulting from the small *b* axis of the microcrystallites. GSAS allows for refinement of preferred orientation using a series of spherical harmonics.[53] Thus, before performing a Rietveld refinement of the crystal structure, a sixth-order spherical harmonic was refined. The analysis produced a texture value of 1.2, and the angular distribution along the 001, 100, and 010 crystal faces indicated a funnel-shaped packing scenario. The inclusion of the texture model significantly improved the low-angle fit of the data, and the structure solution using XRD proceeded.

Further XRD Refinement using Bond Distance and Angle Restraints. Restraint files were created for the bond distances and the angles between bonds based on the standard experimental values for each of the atomic configurations (i.e., sp^2 versus sp^3). Due to the nonatomic resolution of the data (minimum usable *d* spacing of 1.5 Å), it seemed prudent to restrain the atoms to the known distances in the refinement than to let them wholly vary. The A- and B-ring atoms (including the hydrogens) remained planar after several rounds of refinement; therefore, planar restraints for these two features were added to ease convergence. A restraint on the chiral center volume (2.5) was added for the C2 and C3 atoms. There are 101 restraints for this structure—37 bonds, 60 angles, 2 planes, and 2 chiral centers. Once the atomic coordinates of the (+)-catechin crystal structure were identified, difference density maps were created by GSAS to locate water molecules in the solvent. Rapid XRD analysis times of less than 10 min ensured retention of all waters of hydration, and five water molecules were identified, which are integral to the hydrogen bond scaffolding. The data did not allow for a detailed temperature factor analysis at this point, but the U_{iso} values of the heavy atoms, the waters, and hydrogens were collectively evaluated with values of 0.0298, 0.0811, and 0.0228, respectively.

Orienting OH Hydrogens with SSNMR Data. X-ray powder diffraction data are insensitive to proton locations because hydrogen atoms scatter poorly. Thus, positions of hydrogens in C−H bonds are usually inferred from geometry. More problematic are OH protons, because neighboring moieties often suggest more than one orientation for these H's to optimize hydrogen bonding. These intermolecular hydrogen bond dictated orientations can be energetically less favorable than conformations obtained from consideration of a single molecule under vacuum. Previous SSNMR analysis, which can probe H positions, has demonstrated that OH conformations can be established with an accuracy of ±11° in the dihedral angle using tensor principal values.[56,28e] This approach compares the three experimental tensor principal values measured at each ^{13}C site with corresponding computed values from conformationally varied model structures. In catechin, such experimental tensor data (described in Table 2) were acquired using the FIREMAT technique.[34] Ten model structures were prepared and computed ^{13}C tensor values compared to establish OH proton orientations. Ingold has previously established that phenolic O−H protons invariably lie in or very near the plane of the aromatic ring.[57] Even steric factors due to bulky ortho substituents (e.g., 2,6-di-*tert*-butyl-4-substituted phenols) do not significantly alter this coplanarity. Therefore, all models considered initially placed the phenolic proton in the plane of the aromatic ring. Optimal orientations were established by a geometry refinement using

(52) Pawley, G. S. *J. Appl. Crystallogr.* **1981**, *14*, 357.
(53) Larson, A. C.; Von Dreele, R. B. General Structure Analysis System (GSAS); Los Alamos National Laboratory Report LAUR 86-748, 2000.
(54) (a) Stephens, P. W. *J. Appl. Crystallogr.* **1999**, *32*, 281. (b) Finger, L. W.; Cox, D. E.; Jephcoat, A. P. *J. Appl. Crystallogr.* **1994**, *27*, 892.
(55) Pagola, S.; Stephens, P. W. *Mater. Sci. Forum* **2000**, *321*−*324*, 40–45.
(56) Harper, J. K.; Mulgrew, A. E.; Li, J. Y.; Barich, D. H.; Strobel, G. A.; Grant, D. M. *J. Am. Chem. Soc.* **2001**, *123*, 9837.
(57) (a) Ingold, K. U.; Taylor, D. R. *Can. J. Chem.* **1961**, *39*, 471. (b) Ingold, K. U.; Taylor, D. R. *Can. J. Chem.* **1961**, *39*, 481. (c) Wright, J. S.; Carpenter, D. J.; Mckay, D. J.; Ingold, K. U. *J. Am. Chem. Soc.* **1997**, *119*, 4245.

Table 2. ^{13}C Principal Values (ppm) of Catechin 4.5-Hydrate[a]

position	δ_{iso} ^{13}C	δ_{11}	δ_{22}	δ_{33}
2	81.37	91.7	91.7	60.7
3	66.07	82.1	82.1	34.0
4	27.40	40.6	23.2	18.2
4a	100.52	159.3	121.5	20.8
5[b]	155.81	233.7	165.8	68.0
6	97.25	151.0	110.9	29.9
7[b]	155.80	236.4	163.2	67.7
8	93.79	149.8	102.8	28.8
8a	153.85	233.9	159.0	68.7
1′	128.97	216.7	154.0	16.2
2′	116.19	190.4	139.6	18.5
3′	145.12	217.1	154.5	63.7
4′	144.43	212.1	157.6	63.5
5′	117.76	196.1	134.1	23.0
6′	125.31	221.6	132.0	22.4

[a] Average error in measured principal values is ±0.9 ppm based on analyses described in the Experimental Section. [b] The ^{13}C signals for these carbons are degenerate, and the HETCOR ^{1}H shifts are used to obtain the assignments shown. Specifically, the lower frequency portion of the ^{13}C signal near 155.8 ppm receives magnetization from the C8 proton, indicating that C7 is the more shielded region of the overlapped peak.

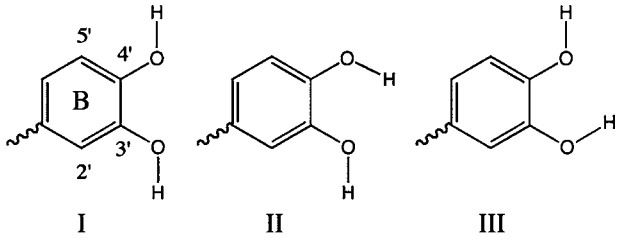

Figure 5. The three OH hydrogen orientations considered for the B-ring. Structure II gave the best fit to experimental data, with structures I and III rejected with high statistical confidence. The A- and C-rings are omitted here because varying the OH protons in these rings had only a small influence (less than 1 ppm) on all B-ring tensor values.

an energy minimization procedure. The specific model structures evaluated are described below. All computed ^{13}C tensor values are included in the Supporting Information.

The OH proton orientations in the B-ring were modeled first. This choice allows conformational uncertainties at other OH hydrogens to be ignored because such sites are several bonds removed and therefore have only a minor influence on computed tensor values in the B-ring. Three model structures were evaluated to locate the OH protons in the B-ring (shown in Figure 5), and only carbons from the B-ring were included in the statistical comparison. Conformations of all OH's in the A- and C-rings were arbitrarily set due to their negligible influence. Model II was retained as the most probable structure, with models I and III rejected at the 83% and 85% confidence levels, respectively. Independent support for model II was found in the HETCOR data, where a strong C3′O$-^{1}$H $\rightarrow$ ^{13}C2′ correlation was observed at a contact time of 210 μs.

An evaluation of OH orientations in the A-ring included four conformations (displayed in Figure 6). In all models, the B-ring OH conformations established previously for model II were retained. Computed tensors for these structures were compared to experimental data from all A-ring carbons, and model IV was eliminated as a probable structure at the 94% confidence level. The three remaining structures (V−VII) were statistically indistinguishable, with all giving high-quality fits. Fortunately, further selection among these structures was possible on the basis of the HETCOR ^{1}H/^{13}C dipolar coupling correlations.

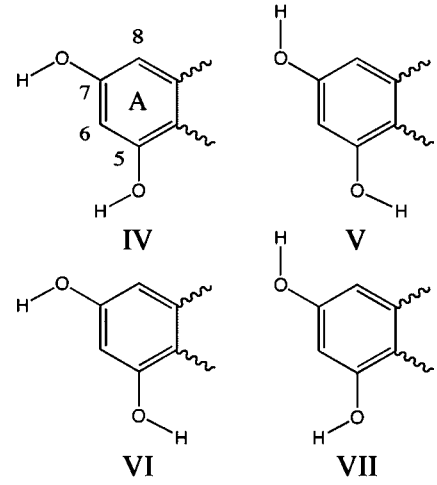

Figure 6. The four A-ring OH hydrogen orientations evaluated. Model VII gave the best fit to experimental data. Model IV was rejected (94% confidence level) on the basis of a poor fit to tensor data from all A-ring carbons. Models V and VI were rejected on the basis of the observation of a C5O$-^{1}$H $\rightarrow$ ^{13}C6 transfer in the experimental HETCOR data indicating a C5OH hydrogen directed toward the C6 carbon. Omission of the B- and C-rings in this figure reflects the fact that conformational variations in these rings had little effect on tensor values in the A-ring. In all calculations, the complete B- and C-rings were included.

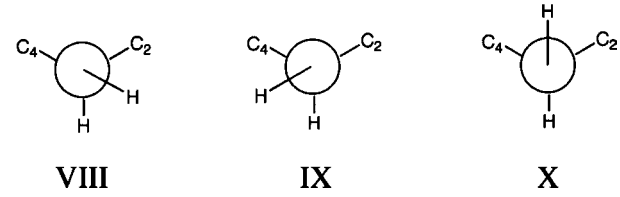

Figure 7. Newman projections of conformational models investigated at the C3OH hydrogen. Model X was eliminated with high statistical confidence of 87%, but models VIII and IX gave equal quality fits and were both retained as probable conformations. Subsequent refinement using X-ray diffraction data found dynamic disorder at C3 and indicated a structure consisting of a 50/50 fractional occupancy of VIII and IX.

Specifically, a C5O$-^{1}$H $\rightarrow$ ^{13}C6 transfer was observed at a contact time of 90 μs, indicating that the C5OH proton is oriented toward C6. Of the three remaining structures, only model VII has this orientation. Notably, model VII is also consistent with the previously described observation that C6 and C8 receive magnetization from the C5O$-^{1}$H and C7O$-^{1}$H hydrogens, respectively, during short cross-polarization periods.

Modeling the OH orientation at C3 involved three structures prepared by placing the protons at the three staggered positions around the C3−O bond (shown in Figure 7). This choice reflects the fact that staggered conformations are usually energetically preferred for C−O bonds involving sp^3 carbons.[58] All OH orientations in the A- and B-rings were retained at the best-fit positions previously described. Comparison to computed tensors eliminated model X at the 87% confidence level. The remaining structures (models VIII and IX) both gave high-quality fits, which were statistically equivalent. Further selectivity from HETCOR correlations was not obtained, because the ^{1}H signal from the C3OH produced no ^{1}H/^{13}C correlations with neighboring sites such as C2 and C4. Models VIII and IX were therefore both retained as feasible structures.

In addition to the prediction of OH hydrogen conformation, SSNMR provides estimations of relative hydrogen bond strengths

(58) Lowe, J. P. *Prog. Phys. Org. Chem.* **1968**, *6*, 1.

at certain OH sites.[59] Phenolic OH proton shifts reflect both the strength of hydrogen bonding at the OH and the aromatic substitution pattern.[60] When two phenols have the same substitution pattern and similar substituents, variations in the O^1H shifts primarily reflect differences in hydrogen bond strength, with higher frequency shifts indicating stronger hydrogen bonding.

In catechin 4.5-hydrate, the two A-ring OH's have similar substitution environments and O^1H shifts are likely to reflect differences in hydrogen bond strength. The strongest hydrogen bonding is predicted to occur at C7, where a ^1H shift of 9.3 ppm is observed. An O^1H shift of 8.4 ppm at C5 indicates a weaker hydrogen bond. Similar comparisons can be made in the B-ring at C3′ and C4′, where respective O^1H isotropic shifts of 8.0 and 9.3 ppm are observed. The C4′O-H is therefore predicted to experience the strongest hydrogen bonding among B-ring OH's.

XRD Confirmation of OH Orientations and Elucidation of Hydrogen Bonding. The feasibility of all SSNMR-predicted OH hydrogen orientations was verified by refining the XRD crystal structure with the addition of the SSNMR determined OH hydrogen orientations. While the XRD refinement could not confirm the hydrogen positions themselves, the stability of the water oxygen locations with these conformations suggested that the OH positions were correct. At C3, refinement revealed disorder with contributions to the structure from models VIII and IX with a 50/50 fractional occupancy.

Disorder at C3 caused difficulty in tracing the hydrogen-bonding connectivity though the lattice. Bonds that represent split occupancies propagate this disorder into other parts of the structure. Unequivocal determination of the hydrogen bond network was therefore not achieved among the waters themselves or at C4′OH, C3′OH, or C3OH. Nevertheless, at the interface between catechin and the water channel, the following donor and acceptor combinations can be made with confidence. On the A-ring, the C7-OH donates a proton to the nearby water oxygen (O2). The C5-OH is a donor to the oxygen at C7 in a neighboring catechin and also interacts with either the HO3H or HO4H water, depending upon the conformation of the C3O-H at a given time. The B-ring contains interactions at C4′-OH with both HO1H and C3′-OH. The C3′OH also interacts with the C3OH of a neighboring molecule. The water oxygen at the special Wyckoff position (O5) is surrounded by water molecules and does not interact with any nearby catechin molecules. This water is easily lost upon drying, leading to more extensive water loss and a phase change. Hence, HO5H serves as an essential structural component for this lattice.

These hydrogen-bonding assignments taken together with the previously described SSNMR observation of rapid C5O-^1H to $^{13}C6$ and C7O-^1H to $^{13}C8$ HETCOR transfers (i.e., 90 μs) suggests that the C5OH and C7OH hydrogens exist largely in a single conformation. The HETCOR data at C3′ and C4′ are less clear where only a slow transfer from C3′O-^1H to $^{13}C2$' is observed and *no* C4'O$-^1H$ to $^{13}C3'$ transfer is detected. These observations allow for the possibility of disorder at the C3′OH and C4′OH protons. Nevertheless, the close match between experimental and model ^{13}C tensor data at these sites indicates that the conformation shown in Figure 5 (structure II) represents the largest population.

It should be noted that since XRD data provide no method for refining hydrogen positions, the coordinates reported in the CIF file (available as Supporting Information) for hydrogens are those obtained from an ab initio refinement of catechin H atoms performed while keeping heavier atoms frozen at XRD positions. Prior work has demonstrated that inaccurate hydrogen positions result in poor fits between experimental and computed ^{13}C tensor data.[61] In catechin, the close match of these values implies that the reported hydrogen positions are accurate. No hydrogen positions are reported for waters due to disorder.

Refinement of XRD Heavy-Atom Positions with SSNMR ^{13}C Tensor Values. NMR tensor values have recently been demonstrated to provide a remarkably sensitive means of evaluating the quality of a proposed powder or fiber diffraction structure.[28e,h,j] Structural errors are indicated by a large scatter in a linear plot of experimental principal values versus tensors computed from the diffraction coordinates. Because tensor data are available at individual molecular sites, structural errors can be precisely located and corrected. Presently, tensor data have been used to refine heavy-atom coordinates in the zeolite Sigma-2 (^{29}Si data),[28h] in uniformly ^{13}C labeled cellulose I_α,[28j] and in a ^{13}C study of a natural abundance fungal product, ambuic acid.[28e] In the case of Sigma-2, the SSNMR refinement of the XRD structure resulted in a molecular structure of a quality comparable to the known single-crystal diffraction model.[28h] Stimulated by these results, a further refinement of the catechin structure was pursued using the XRD-refined coordinates.

The structure of catechin initially obtained from the XRD analysis was further refined by retaining all dihedral angles at the values determined and then refining bond lengths and valence angles by an energy minimization procedure. This approach has previously been demonstrated to significantly improve the fit between experimental and computed SSNMR shift tensor values while retaining a high-quality XRD fit.[28e] In catechin, this refinement reduced the error in the SSNMR fit from 11.33 to 4.84 ppm; however, this process omits the water molecules present in the lattice and is therefore incomplete. The XRD data was used to relocate waters using electron density maps. The resulting structure containing all waters and the refined catechin molecule had an increased XRD error of 0.119 (wRp) versus the 0.067 obtained before the refinement step, suggesting that a new Rietveld refinement of the complete structure was required. An iterative process was therefore pursued involving XRD refinement of the complete structure (catechin with waters) followed by a new ab initio refinement of bond lengths and valence angles of catechin with the waters excluded. The refinement converged to a common structure in three steps (see Figures 8−10). A more detailed description of this refinement and errors for each step (SSNMR and XRD) is given as Supporting Information. The CIF structure reported in the Supporting Information is the structure obtained after this three-step refinement. The agreement between experimental and computed SSNMR data in this final structure is nearly identical with that observed in closely related aromatic compounds when

(59) (a) Wu, G.; Freure, C. J.; Verdurand, E. *J. Am. Chem. Soc.* **1998**, *120*, 13187. (b) Sears, R. E. J.; Kaliaperumal, R. *J. Chem. Phys.* **1990**, *93*, 2959. (c) Berglund, B.; Vaughan, R. W. *J. Chem. Phys.* **1980**, *73*, 2037. (d) Ditchfield, R. *J. Chem. Phys.* **1976**, *65*, 3123. (e) Kaliaperumal, R.; Sears, R. E. J.; Ni, Q. W.; Furst, J. E. *J. Chem. Phys.* **1989**, *91*, 7387. (f) Rohlfing, C. M.; Allen, L. C.; Ditchfield, R. *J. Chem. Phys.* **1983**, *79*, 4958.

(60) Pretsch, E.; Clerc, T.; Seibl, J.; Simon, W. *Structure Determination of Organic Compounds: Tables of Spectral Data*; Springer-Verlag: Berlin, 1989.

(61) (a) Liu, F.; Orendt, A. M.; Alderman, D. W.; Grant, D. M. *J. Am. Chem. Soc.* **1997**, *119*, 8981. (b) Grant, D. M.; Liu, F.; Iuliucci, R. J.; Phung, C. G.; Facelli, J. C.; Alderman, D. W. *Acta Crystallogr.* **1995**, *B51*, 540.

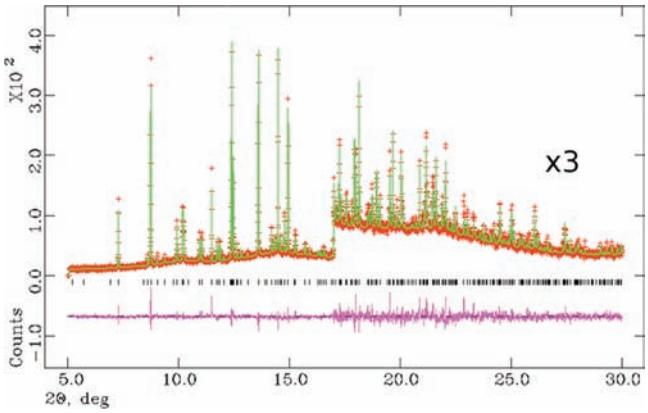

Figure 8. Figure of final fit to XRD data with the 17−30° region (including the difference curve) at a 3× zoom to clearly show the higher angle data. The data are red crosses; the fit is a green line. The reflection positions are described by black tick marks, and the difference curve is shown in magenta.

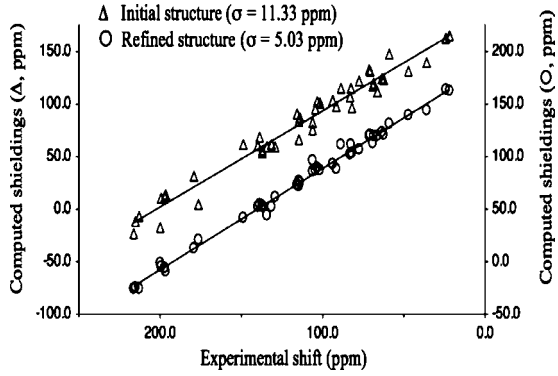

Figure 9. The initial structure, solved using XRD heavy-atom positions and SSNMR OH hydrogen orientations, had excellent agreement with diffraction data ($wR_p = 0.067$) but gave a poor fit of computed tensor principal values with experimental data (△). This large error in SSNMR fit indicated that further refinement was possible. A significant improvement in the fit (○) was obtained in the final refinement by adjusting bond lengths and valence angles computationally, while holding dihedral angles constant at XRD values. Computed shieldings at sp^2 sites have systematic errors that are less problematic at sp^3 carbons (see the Experimental Section). The trend lines shown here are intended to show only overall improvement in the correlation and do not reflect these systematic differences.

tensors are computed from coordinates of high-quality single-crystal structures.[45b]

The feasibility of the bond lengths and valence angles in the structure obtained from the iterative refinement process is independently confirmed by a comparison with the X-ray structure of a closely related flavonoid. Tetra-*O*-methylcatechin[19] has an identical substitution pattern and stereochemistry in the A-, B-, and C-rings and was therefore chosen for comparison. The refined catechin structure closely matches tetra-*O*-methylcatechin in bond lengths between non-hydrogen atoms with a standard deviation of ±0.0154 Å. This comparison includes all bonds in the three rings and the C−O bonds at C3, C5, C7, C3′, and C4′. Likewise, the valence angles in catechin accurately reflect those in tetra-*O*-methylcatechin with a standard deviation of ±1.80° measured for the non-hydrogen atoms listed above.

Recent work suggests that further improvements to atomic positions may have been achieved by theoretical methods that

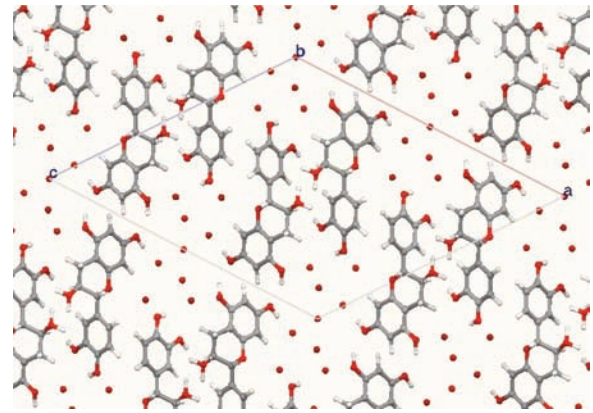

Figure 10. Final atomic coordinate positions for the (+)-catechin 4.5-hydrate looking down the *b* axis. The structure is shown as a ball-and-stick model with the carbons in gray, oxygen atoms in red, and hydrogens in white. The unit cell is displayed as a box with the *a* axis along *b*−*a* and the *c* axis along *b*−*c*. Symmetry-related molecules within the *x*−*z* plane are displayed. Hydrogens are omitted from all waters due to disorder. The disorder at the C3O-H hydrogen is indicated by including both occupied H positions.

account for lattice effects.[42c,62] These recently introduced techniques enable geometry refinements that include lattice structure[41b,f] and have been demonstrated to provide very accurate structures. In the case of catechin 4.5-hydrate, however, the complete set of atomic coordinates needed to perform such a calculation are unavailable due to the omission of hydrogens on waters. Nevertheless, the close agreement between experimental and computed SSNMR tensors for the final structure taken together with the close match to X-ray bond lengths and valence angles of tetra-*O*-methylcatechin indicates that the refined catechin structure is already reasonably accurate. Further refinement by lattice-including methods is therefore expected to produce relatively minor changes.

Prior work has demonstrated that refinement of only hydrogens can significantly improve the fit between computed and experimental SSNMR tensors.[61] Since hydrogens were also optimized during the iterative refinement process described, a separate analysis was performed to determine what portion of the improvement was due to hydrogen optimization. Optimal hydrogen positions were determined by holding heavy atoms rigid at the initially determined XRD-determined positions (i.e., before any bond length or valence angle refinement) and allowing only hydrogens to adjust via energy minimization. Tensors (^{13}C) were then computed using the coordinates of the modified structure. This hydrogen refinement altered the computed error by only 0.48 ppm relative to the structure before refinement. It may therefore be concluded that roughly 93% of the improvement in the SSNMR error comes from refinement of non-hydrogen atoms.

Conclusion

The first crystal structure for (+)-catechin 4.5-hydrate is obtained using XRD-determined heavy-atom positions and OH dihedral angles established from SSNMR data. The tendency of catechin 4.5-hydrate to rapidly dehydrate and change phases is demonstrated and may explain the inability to characterize catechin previously. The unusual step of refining bond lengths and valence angles through a SSNMR ^{13}C tensor analysis was

(62) Olsen, R. A.; Struppe, J.; Elliott, D. W.; Thomas, R. J.; Mueller, L. J. *J. Am. Chem. Soc.* **2003**, *125*, 11785.

undertaken using the proposed XRD structure. This process retains XRD dihedral angles and has been demonstrated to significantly improve the fit of SSNMR tensor data. This final modification retains a high-quality fit to XRD data and thus represents an improvement to the structure.

Acknowledgment. We thank Dr. Yuegang Zhang for assistance in analyzing earlier synchrotron powder diffraction data for catechin 4.5-hydrate. Funding for this work was provided by a grant from the National Institutes of Health (Grant No. 5R01GM008521-46). The computational resources for this project have been provided by the National Institutes of Health (Grant No. NCRR 1 S10 RR17214-01) on the Arches Metacluster, administered by the University of Utah Center for High Performance Computing. The use of the APS, beamline 11-BM, was supported by the U.S. Department of Energy, Office of Science, Office of Basic Energy Sciences, under contract number DE-AC02-06CH11357. Cover art was furnished by Dr. Elizabeth M. Heider.

Supporting Information Available: A CIF file giving crystal data for the final (+)-catechin 4.5-hydrate structure and figures, text, and tables giving solution NMR shifts (^{13}C and ^{1}H) for (+)-catechin in D_2O, plots of all ^{1}H/^{13}C HETCOR SSNMR spectra, computed ^{13}C shielding tensor principal values for model structures I−X, a table of the errors for each step in the refinement of XRD heavy atom positions with SSNMR ^{13}C tensor values, and the full Gaussian citation (complete ref 38). This material is available free of charge via the Internet at http://pubs.acs.org.

JA907671P